



Two-photon deep-tissue spatially resolved mitochondrial imaging using membrane potential fluorescence fluctuations

KAYVAN FOROUHESH TEHRANI,¹ EMILY G. PENDLETON,¹ WILLIAM M. SOUTHERN,² JARROD A. CALL,² AND LUKE J. MORTENSEN^{1,3,*}

¹Regenerative Bioscience Center, Rhodes Center for ADS, University of Georgia, Athens, GA 30602, USA

²Department of Kinesiology, University of Georgia, Athens, GA 30602, USA

³School of Materials, Chemical, and Biomedical Engineering, University of Georgia, Athens, GA 30602, USA

*luke.mortensen@uga.edu

Abstract: Cell metabolism and viability are directly reflected in their mitochondria. Imaging-based analysis of mitochondrial morphological structure, size and dynamic characteristics can therefore provide critical insight into cell function. However, mitochondria are often very abundant, and due to their close to diffraction-limit size, it is often non-trivial to distinguish a tubular or large mitochondrion from an ensemble of punctate mitochondria. In this paper, we use membrane potential dependent fluorescence fluctuations of individual mitochondria to resolve them using an approach similar to single molecule localization microscopy. We use 2-photon microscopy to image mitochondrial intensity fluctuations at 200 μm deep inside an intact in-vivo mouse soleus muscle. By analyzing the acquired images, we can reconstruct images with an extra layer of information about individual mitochondria, separated from their ensemble. Our analysis shows a factor of 14 improvement in detection of mitochondria.

© 2017 Optical Society of America under the terms of the [OSA Open Access Publishing Agreement](#)

OCIS codes: (180.4315) Nonlinear microscopy; (190.4180) Multiphoton processes; (170.2520) Fluorescence microscopy; (100.6640) Superresolution; (100.0100) Image Processing; (170.3880) Medical and biological imaging

References and links

1. K. G. Hales and M. T. Fuller, "Developmentally Regulated Mitochondrial Fusion Mediated by a Conserved, Novel, Predicted GTPase," *Cell* **90**(1), 121–129 (1997).
2. Z. Li, K. Okamoto, Y. Hayashi, and M. Sheng, "The importance of dendritic mitochondria in the morphogenesis and plasticity of spines and synapses," *Cell* **119**(6), 873–887 (2004).
3. P. J. Hollenbeck and W. M. Saxton, "The axonal transport of mitochondria," *J. Cell Sci.* **118**(23), 5411–5419 (2005).
4. Y.-C. Hsu, Y.-T. Wu, T.-H. Yu, and Y.-H. Wei, "Mitochondria in mesenchymal stem cell biology and cell therapy: From cellular differentiation to mitochondrial transfer," *Semin. Cell Dev. Biol.* **52**, 119–131 (2016).
5. P. Mishra, G. Varuzhanyan, A. H. Pham, and D. C. Chan, "Mitochondrial Dynamics is a Distinguishing Feature of Skeletal Muscle Fiber Types and Regulates Organellar Compartmentalization," *Cell Metab.* **22**(6), 1033–1044 (2015).
6. E. Frazier Ann, C. Kiu, D. Stojanovski, J. Hoogenraad Nicholas, and T. Ryan Michael, "Mitochondrial morphology and distribution in mammalian cells," in *Biological Chemistry*, (2006), p. 1551.
7. D.-F. Suen, K. L. Norris, and R. J. Youle, "Mitochondrial dynamics and apoptosis," *Genes Dev.* **22**(12), 1577–1590 (2008).
8. P. K. Kennady, M. G. Ormerod, S. Singh, and G. Pande, "Variation of mitochondrial size during the cell cycle: A multiparameter flow cytometric and microscopic study," *Cytometry A* **62**(2), 97–108 (2004).
9. M. Karbowski, K. L. Norris, M. M. Cleland, S.-Y. Jeong, and R. J. Youle, "Role of Bax and Bak in mitochondrial morphogenesis," *Nature* **443**(7112), 658–662 (2006).
10. S.-H. Shim, C. Xia, G. Zhong, H. P. Babcock, J. C. Vaughan, B. Huang, X. Wang, C. Xu, G.-Q. Bi, and X. Zhuang, "Super-resolution fluorescence imaging of organelles in live cells with photoswitchable membrane probes," *Proc. Natl. Acad. Sci. U.S.A.* **109**(35), 13978–13983 (2012).
11. J. Xu, K. F. Tehrani, and P. Kner, "Multicolor 3D Super-resolution Imaging by Quantum Dot Stochastic Optical Reconstruction Microscopy," *ACS Nano* **9**(3), 2917–2925 (2015).
12. L. Shao, P. Kner, E. H. Rego, and M. G. Gustafsson, "Super-resolution 3D microscopy of live whole cells using structured illumination," *Nat. Methods* **8**(12), 1044–1046 (2011).

13. M. Brunstein, K. Wicker, K. Héroult, R. Heintzmann, and M. Oheim, "Full-field dual-color 100-nm super-resolution imaging reveals organization and dynamics of mitochondrial and ER networks," *Opt. Express* **21**(22), 26162–26173 (2013).
14. E. Betzig, G. H. Patterson, R. Sougrat, O. W. Lindwasser, S. Olenych, J. S. Bonifacino, M. W. Davidson, J. Lippincott-Schwartz, and H. F. Hess, "Imaging Intracellular Fluorescent Proteins at Nanometer Resolution," *Science* **313**(5793), 1642–1645 (2006).
15. S. Chalmers, C. D. Saunter, J. M. Girkin, and J. G. McCarron, "Age decreases mitochondrial motility and increases mitochondrial size in vascular smooth muscle," *J. Physiol.* **594**(15), 4283–4295 (2016).
16. S. Chalmers, C. D. Saunter, J. M. Girkin, and J. G. McCarron, "Flicker-assisted localization microscopy reveals altered mitochondrial architecture in hypertension," *Sci. Rep.* **5**(1), 16875 (2015).
17. T. Dertinger, R. Colyer, G. Iyer, S. Weiss, and J. Enderlein, "Fast, background-free, 3D super-resolution optical fluctuation imaging (SOFI)," *Proc. Natl. Acad. Sci. U.S.A.* **106**(52), 22287–22292 (2009).
18. R. C. Scaduto, Jr. and L. W. Grotyohann, "Measurement of mitochondrial membrane potential using fluorescent rhodamine derivatives," *Biophys. J.* **76**(1), 469–477 (1999).
19. B. Glancy, L. M. Hartnell, D. Malide, Z.-X. Yu, C. A. Combs, P. S. Connelly, S. Subramaniam, and R. S. Balaban, "Mitochondrial reticulum for cellular energy distribution in muscle," *Nature* **523**(7562), 617–620 (2015).
20. S. W. Perry, J. P. Norman, J. Barbieri, E. B. Brown, and H. A. Gelbard, "Mitochondrial membrane potential probes and the proton gradient: a practical usage guide," *Biotechniques* **50**(2), 98–115 (2011).
21. K. M. Abdel-Hamid and M. Tymianski, "Mechanisms and effects of intracellular calcium buffering on neuronal survival in organotypic hippocampal cultures exposed to anoxia/aglycemia or to excitotoxins," *J. Neurosci.* **17**(10), 3538–3553 (1997).
22. D. G. Nicholls and M. W. Ward, "Mitochondrial membrane potential and neuronal glutamate excitotoxicity: mortality and millivolts," *Trends Neurosci.* **23**(4), 166–174 (2000).
23. K. F. Tehrani, E. G. Pendleton, C. P. Lin, and L. J. Mortensen, "Deep tissue single cell MSC ablation using a fiber laser source to evaluate therapeutic potential in osteogenesis imperfecta," in 2016), 97110D–97110D–97118.
24. L. H. Mbye, I. N. Singh, P. G. Sullivan, J. E. Springer, and E. D. Hall, "Attenuation of acute mitochondrial dysfunction after traumatic brain injury in mice by NIM811, a non-immunosuppressive cyclosporin A analog," *Exp. Neurol.* **209**(1), 243–253 (2008).
25. K. Ito, R. Turcotte, J. Cui, S. E. Zimmerman, S. Pinho, T. Mizoguchi, F. Arai, J. M. Runnels, C. Alt, J. Teruya-Feldstein, J. C. Mar, R. Singh, T. Suda, C. P. Lin, P. S. Frenette, and K. Ito, "Self-renewal of a purified Tie2+ hematopoietic stem cell population relies on mitochondrial clearance," *Science* **354**(1), 1156 (2016).

1. Introduction

Mitochondria are organelles that provide energy for the cell, and have a regulatory role for cellular metabolism. Mitochondrial dynamics are of central importance in cell processes that occur during development [1], throughout the brain and nervous system [2, 3], in therapeutic stem cells [4], and during muscle function [5]. During a cell's life cycle mitochondria move along microtubules and actin filaments, and go through processes such as fission and fusion at various speeds depending on their environment, cell health and differentiation [6–8]. Therefore, their morphology, structure, geometrical shape, tubularity, size, abundance and dynamic features such as speed and rate of fission and fusion (Fig. 1), can be used as indicators of the health and metabolism of a cell or tissue [1, 7, 9].

In recent years, optical fluorescent super-resolution microscopy of mitochondria [10–12] has enabled visualizing interactions within their highly dynamic and regulated networks and processes. These methods include 3D structured illumination microscopy (SIM) with a 120 nm lateral and 360 nm axial resolution [12], TIRF-SIM [13], and 2D stochastic optical reconstruction microscopy (STORM) with 40 nm lateral resolution [10] in living cells, and *in vitro* [11]. One challenge in imaging mitochondria is their sub-diffraction-limit size (200–500 nm) and their abundance in the cytoskeleton [8, 14, 15]. They often exist in groups of multiple mitochondria in contiguous layers and close proximity, which makes it non-trivial to distinguish a tubular mitochondrion from an ensemble of punctate mitochondria.

Super-resolution techniques can overcome this challenge; but constraints such as the large number of frames required to produce a high resolution (laterally and axially) image reduce their utility in the fast-evolving dynamic environment of the cell. Recently, a method that uses natural fluorescence fluctuations of mitochondria has emerged called fluctuation assisted localization microscopy (FaLM) [16], which can be exploited for simple and rapid analysis of these sub-diffraction sized closely positioned mitochondria. The method uses principles

similar to single molecule localization microscopy [10, 11], and SOFI [17], to enhance the resolving power. FaLM requires a series of images taken with sub-diffraction-limit pixel size from a sample that is fluorescently labeled with a membrane potential sensitive probe such as Tetramethylrhodamine ethyl/methyl ester (TMRE/TMRM), Rhodamine 123 [18].

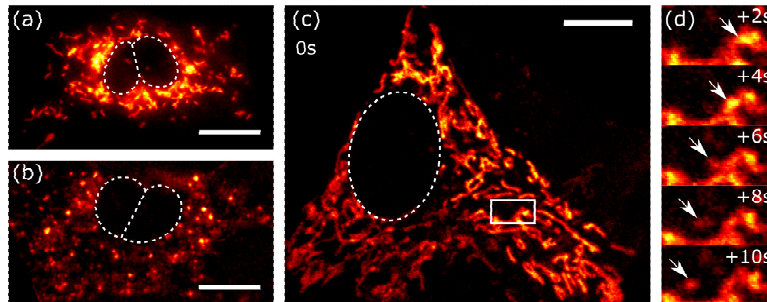


Fig. 1. *In vitro* images of tubular and punctate mitochondria of mesenchymal stem cells, shown in (a) and (b), respectively. The cells are labeled with mitotracker green, and imaged using single photon excitation. We show motion of single mitochondria in a large assembly in (c), by 2-photon imaging of MSC mitochondria stained with TMRE. The zoomed-in timelapse of the boxed area in (c) are shown in (d). Scale bars are 10 μ m. The boxed area is 6.35 x 3.33 μ m.

The FaLM technique has been applied to intact samples using single photon excitation fluorescence microscopy. To understand mitochondrial dynamics *in vivo*, it is important to determine applicability of the method to cell organelles located at deeper planes within a tissue. The main challenge here is that biological tissues are scattering, and therefore single photon microscopy past the mean-free-path becomes dominated by optical aberrations and loses resolution and accuracy. One solution to this problem is exploiting longer wavelength excitation light of multi-photon microscopy, to benefit from its longer penetration depth, with lower deviation from diffraction-limited resolution [19]. In this paper we present FaLM using 2-photon excitation (2p-FaLM), which has intrinsic optical sectioning and uses long mean-free path near-infrared or infrared light. We first applied this technique to an *in vitro* monolayer of living mesenchymal stem cells (MSCs), by staining the cells with TMRE and imaging at video rate. We then imaged at 200 μ m depth from the surface into an *in vivo* mouse soleus muscle. The soleus muscle is a posterior crural muscle located in the mouse hindlimb that contributes to plantar flexion torque about the ankle joint. The soleus muscle is a mitochondria-rich slow-twitch, oxidative tissue that primarily uses oxidative phosphorylation to generate adenosine triphosphate (ATP). We tested the effect of the uncoupling agent carbonyl cyanide 4-(trifluoromethoxy)phenylhydrazone (FCCP) on the intensity fluctuation rate and duty cycle. We found that mitochondrial flickering occurs under normal physiological conditions, which suggests the potential of mitochondrial flickering for deep-tissue *in vivo* imaging of cell function and health.

2. Membrane potential fluctuations response to physiological condition

During resting state, mitochondria maintain an unequal distribution of ions across the inner mitochondrial membrane. Hydrogen ions are moved from the mitochondrial matrix to the inner membrane space as electrons are passed along the respiratory electron transport chain and this creates an electrochemical gradient (i.e., mitochondrial membrane potential ($\Delta\phi_m$)) harnessed by the F_1/F_0 ATPase to produce ATP. The parameters involved in this process are the proton force Δp (mV), the mitochondrial membrane potential $\Delta\phi_m$, and the mitochondrial pH gradient $\Delta p H_m$ [20], which are related by $\Delta p = \Delta\phi_m - 60\Delta p H_m$ [21, 22]. Using fluorescent probes that are sensitive to membrane potential $\Delta\phi_m$ enables direct measurement of these exchanges. Fluorescent lipophilic cationic dyes such as the TMRE used in this study have been shown to be effective for this purpose; their advantages and disadvantages are discussed

in [20, 22]. Although the fluorescence intensity of the mitochondria fluctuates in normal physiological conditions (Fig. 2), the equation above shows that because the membrane potential is proportional to the difference in the pH, agents such as FCCP, ADP, or oligomycin can be used to induce or inhibit ionic transfer, thereby increasing the rate of membrane potential fluctuation and resultant flickering of fluorescence signal.

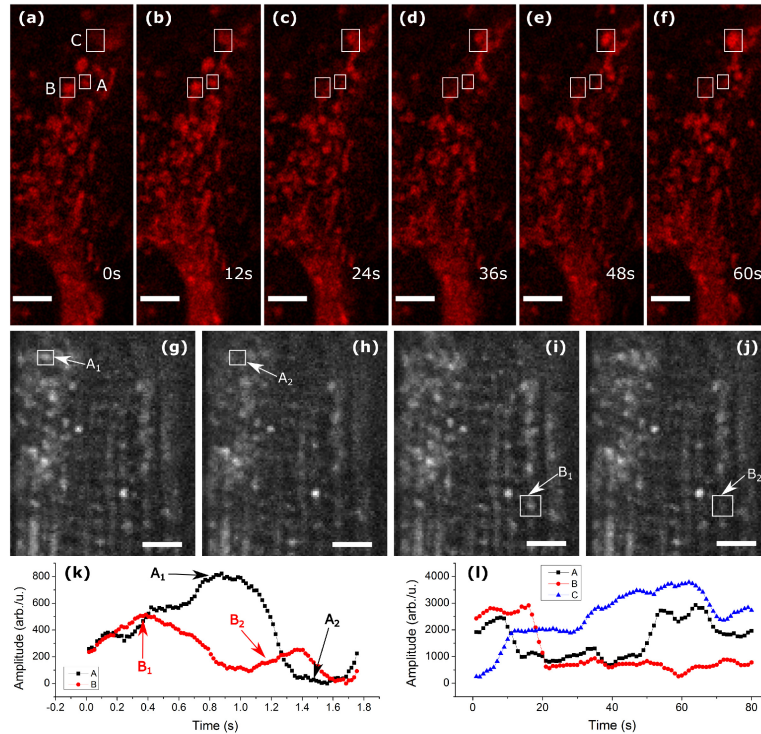


Fig. 2. Mitochondrial blinking. (a-f) show a timelapse of MSC mitochondria intensity fluctuations. (g-j) are timelapse images of mouse soleus muscle. Both samples were stained with TMRE. (k,l) show average intensity in the boxed areas of (g-j), and (a-f), respectively. Scalebars are 5µm.

3. Materials and methods

3.1. Sample conditioning

Wild-type mouse Mesenchymal stem cells (MSCs) were grown on a 35mm Petri dish under standard culture conditions. 20-30 minutes before imaging cells were incubated in 50 nM TMRE in Tyrod's buffer (137 mM NaCl, 2.7 mM KCl, 1.8 mM CaCl₂, 1 mM MgCl₂, 0.2 mM NaH₂PO₄, 12 mM NaHCO₃, 5.5 mM Glucose, pH adjusted to 7.4, and filtered through 0.22 µm syringe filter) at 37° C. For imaging, the petri dish was warmed to 37° C.

3.2. Muscle sample preparation

The soleus muscle was extracted from a C57BL/6 mouse 1 hour before imaging. We permeabilized the muscle in buffer 1 containing (7.23 mM K₂EGTA, 2.77 mM CaK₂EGTA, 20 mM imidazole, 20 mM taurine, 5.7 mM ATP, 14.3 mM PCr, 6.56 mM MgCl₂-6H₂O, 50 mM MES, 100 µg/ml Saponin) for 30 minutes at 4° C. The muscle was then incubated with 50 nM TMRE in a buffer 2 (105 mM MES, 30 mM KCl, 10 mM KH₂PO₄, 5 mM MgCl₂-6H₂O, 0.5 mg/mL BSA, 0.5 M EGTA), for 15 minutes at 4° C. Following incubation with TMRE, the soleus was rinsed in buffer 2 for 15 minutes. The soleus was then removed and glued at proximal and distal tendons to a petri dish. For imaging, the soleus was submerged in

buffer 2 and the following substrates were added to stimulate mitochondrial respiration: glutamate (10 mM), malate (5 mM), ADP (2.5 mM). To increase the rate of fluctuations, FCCP (1 μ M) was added. Animal experiments were done in accordance with UGA IACUC.

3.3. Image reconstruction

We acquired a series of images at a rate appropriate to the condition of blinking, using our 2-photon microscope as explained in [23]. To correct for the observed small amounts of lateral sample movement, we used translation rigid registration. The motion-corrected images were de-noised by Fourier filtering using a circular mask with radius of $2NA/\lambda$, where NA is the numerical aperture of the system, and λ is the wavelength of excitation light. We then subtracted the stack average from individual frames, and calculated the absolute value. This process gives contrast to the mitochondrial intensity fluctuations, and removes static features. We thresholded the images at 20% of the maximum to remove unwanted noise, and applied a temporally encoded coloring scheme to produce spatially resolved images.

For counting of mitochondria in the conventional 2-photon images, we thresholded the image using Otsu's method, and used ImageJ's Analyze Particle module to measure the area and number of mitochondria. In the case of FaLM images, the measurement was done on the color-coded time-series. We consistently used Otsu's method for all thresholdings. Cross sections on the color-coded images are made on their grayscale conversions.

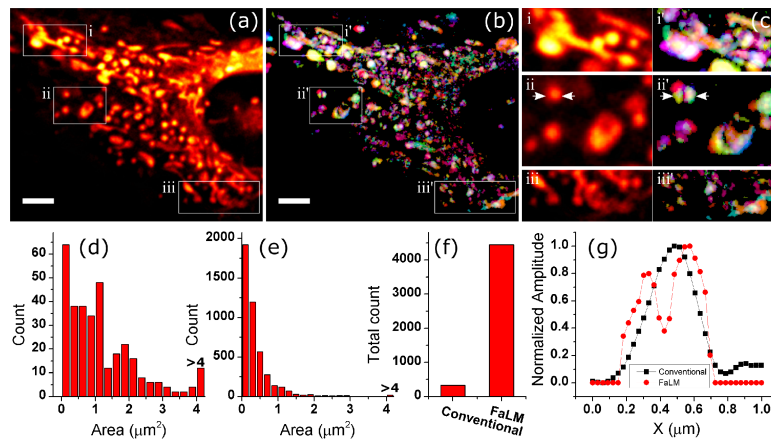


Fig. 3. Stack average (a) and reconstructed image (b) of a cultured MSC in vitro. (c) shows the zoomed in version of boxes in (a,b). (d) and (e) show mitochondria area distribution, for (a) and (b), respectively. The total number of mitochondria is compared in (f). Cross sections shown with arrows in (c) ii and ii' are shown in (g). Black and red lines in (g) represent conventional and FaLM imaging, respectively. Scalebars are 5 μ m.

4. Results and discussion

We first imaged cultured mesenchymal stem cells at 15 frames per second (fps) in the standard physiological buffer. We acquired 3000 images and averaged every 15 frames to improve the signal to noise ratio (SNR), and observe fluctuations in intensity. The averaged image and the reconstructed images are shown in Fig. 3(a), 3(b). With closer inspection (Fig. 3(c)), many mitochondria are resolved from their larger assemblies in the reconstructed images (Fig. 3(g)). We compared the mitochondria area distribution between the original image (Fig. 3(a)) and the FaLM image (Fig. 3(b)), and found a factor of 13 improvement in the number of small mitochondria (Fig. 3(d), 3(e)), and a factor of 14 in the total number of mitochondria (Fig. 3(f)).

The next sample we imaged was mouse soleus muscle. For this sample, we applied FCCP and observed fluctuations at a much faster rate. Therefore, we increased the rate of imaging to 57 fps, and averaged every 10 frames. The muscle contracts in response to the FCCP, so

motion artifact became a limiting factor. We therefore could only use a fraction of images from each acquisition. For the reconstruction of Fig. 4 we used 800 images (before averaging). Comparing the boxed areas in Fig. 4(a), 4(b), we can see 6 individual mitochondria that were blurred into a single spot in the conventional 2-photon image.

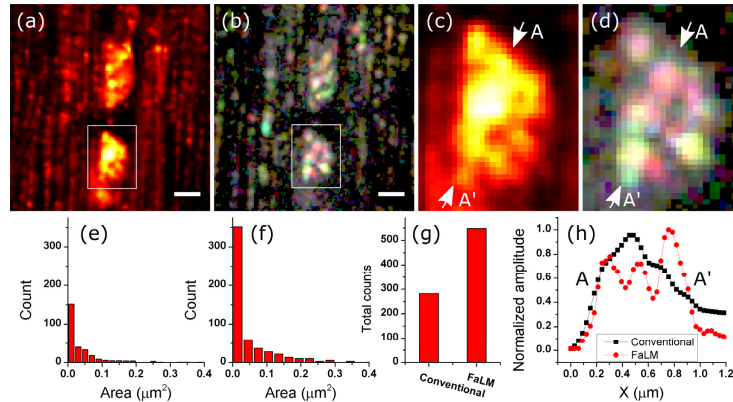


Fig. 4. Mouse Soleus muscle. (a) Stack average. (b) Reconstructed image. (c,d) are the zoomed in version of boxes in (a,b) respectively. (e,f) show the distributions of the mitochondria area for (a,b) respectively. The total number of mitochondria for each mode is shown in (g). A-A' cross sections in (c) and (d) are shown in (h). Black and red lines in (h) represent conventional and FaLM imaging, respectively. Scalebars are 1 μ m.

By comparing the distribution of mitochondria area from the original image (Fig. 4(a)) and the FaLM image (Fig. 4(b)), we find a factor of 2.3 increase in the number of smaller mitochondria (Fig. 4(e), 4(f)), and a factor of 2 increase in the total number of detected mitochondria (Fig. 4(g)). The improvement in resolving of mitochondria is shown by cross sections in Fig. 4(h). The improvement is not as dramatic as for the monolayer of cells, which could be due to the more densely packed cells and the tissue scattering and aberration in thick muscle tissue.

In conclusion, we showed improvement in the mitochondrial resolving power of the 2-photon microscope. Features that were not previously discernable were made visible with short imaging times (\sim 14 sec). The demonstrated algorithm is not computationally expensive, and can easily be applied. We also showed that although mitochondrial decoupling expedites imaging separation of mitochondria, it is not critical. Therefore, deep tissue 2-photon imaging of mitochondrial fluctuations under physiological conditions is a viable strategy to monitor cell metabolic processes in vivo. This analysis can be used for studies of mitochondria involving measurement of other parameters such as oxygen consumption, and electron donor analysis, in areas of neuroscience [24], stem cell biology [25], or skeletal muscle biology [19].

Funding

NSF grant #1706916, Georgia Partners in Medicine REM seed grant, and Georgia Tech Marcus Center Grant to LJM.

Acknowledgement

We would like to thank Dr. Peter Kner for single photon imaging of mitochondria.

Disclosures

The authors declare that there are no conflicts of interest related to this article.